Directed Growth of Poly(isobenzofuran) Films by Chemical Vapor Deposition on Patterned Self-Assembled Monolayers as Templates

Hyun-Goo Choi,[†] John P. Amara,[‡] Timothy M. Swager,[‡] and Klavs F. Jensen*[,†]

Department of Chemical Engineering and Department of Chemistry, Massachusetts Institute of Technology, 77 Massachusetts Avenue, Cambridge, Massachusetts 02139

Received August 1, 2006. In Final Form: November 16, 2006

This paper describes a method to direct the formation of microstructures of poly(isobenzofuran) (PIBF) by chemical vapor deposition (CVD) on chemically patterned, reactive, self-assembled monolayers (SAMs) prepared on gold substrates. We examined the growth dependence of PIBF by deposition onto several different SAMs each presenting different surface functional groups, including a carboxylic acid, a phenol, an alcohol, an amine, and a methyl group. Interferometry, Fourier transform infrared (FT-IR) spectroscopy, X-ray photoelectron spectroscopy (XPS), gel permeation chromatography (GPC), and optical microscopy were used to characterize the PIBF films grown on the various SAMs. Based on the kinetic and the spectroscopic analyses, we suggest that the growth of PIBF is surface-dependent and may follow a cationic polymerization mechanism. Using the cationic polymerization mechanism of PIBF growth, we also prepared patterned SAMs of 11-mercapto-1-undecanol (MUO) or 11-mercaptoundecanoic acid (MUA) by microcontact printing (μCP) on gold substrates as templates, to direct the growth of the PIBF. The directed growth and the formation of microstructures of PIBF with lateral dimensions of 6 μm were investigated using atomic force microscopy (AFM). The average thickness of the microstructures of PIBF films grown on the MUO and the MUA patterns were 400 ± 40 nm and 490 ± 40 nm, respectively. SAMs patterned with carboxylic acid salts (Cu^{2+}, Fe^{2+}, or Ag^{+}) derived from MUA led to increases in the average thickness of the microstructures of PIBF by 10%, 12%, or 27%, respectively, relative to that of control templates. The growth dependence of PIBF on the various carboxylic acid salts was also investigated using experimental observations of the growth kinetics and XPS analyses of the relative amount of metal ions present on the template surfaces.

Introduction

The development of patterning methods for polymeric materials is of interest in such diverse applications as the active elements in light-emitting diodes (LEDs),[1,2] lasers,[3,4] photodiodes,[5,6] and biosensors.[7,8] Conventional patterning routes, such as reactive ion etching (RIE)[9,10] and direct photolithography,[11,12] have been used to create microscopic structures in thin polymer layers. However, there can be undesirable side effects due to the harsh environment of RIE or the photosensitivity of the targeted polymeric materials in direct photolithography. As a result, there are limitations to the use of these approaches for the patterning of polymer thin films.

Microcontact printing (μCP), introduced by Whitesides and co-workers,[13−17] provides a versatile method for the patterning of surfaces at the micro- or the submicrometer scale (feature sizes down to ∼100 nm) with distinct advantages over conventional photolithography; these include the simple, fast, and inexpensive fabrication of patterned surfaces. The μCP of surfaces is achieved through the introduction of localized differences in the surface functional groups using elastomeric stamps that deliver a molecular "ink". The μCP technique has been used to generate patterns of self-assembled monolayers (SAMs) of thiols on gold (or silver)[13−17] and of silanes on silicon substrates.[18,19] Recently, μCP has been extended to produce patterns of a variety of materials, such as cells and biological molecules,[20−27] block copolymers,[28] polyelectrolyte multilayers,[29] dendrimers,[30] con-

* To whom correspondence should be addressed. E-mail: kfjensen@mit.edu. Fax: (617) 258-8224.

[†] Department of Chemical Engineering.

[‡] Department of Chemistry.

(1) Burroughes, J. H.; Bradley, D. D. C.; Brown, A. R.; Marks, R. N.; Macay, K.; Friend, R. H.; Burns, P. L.; Holmes, A. B. *Nature* **1990**, *347*, 539−541.

(2) Braun, D.; Heeger, A. J. *Appl. Phys. Lett.* **1991**, *58*, 1982−1984.

(3) Tessler, N.; Denton, G. J.; Friend, R. H. *Nature* **1996**, *382*, 695−697.

(4) Hide, F.; Diaz-Garcia, M. A.; Schwartz, B. J.; Andersson, M. R.; Pei, Q.; Heeger, A. J. *Science* **1996**, *273*, 1833−1836.

(5) Yu, G.; Gao, J.; Hummelen, J. C.; Wudl, F.; Heeger, A. J. *Science* **1995**, *270*, 1789−1791.

(6) Halls, J. J. M.; Walsh, C. A.; Greenham, N. C.; Marseglia, E. A.; Friend, R. H.; Moratti, S. C.; Holmes, A. B. *Nature* **1995**, *376*, 498−500.

(7) Sirkar, K.; Pishko, M. V. *Anal. Chem.* **1998**, *70*, 2888−2894.

(8) Meiring, J. E.; Schmid, M. J.; Grayson, S. M.; Rathsack, B. M.; Johnson, D. M.; Kirby, R.; Kannappan, R.; Manthiram, K.; Hsia, B.; Hogan, Z. L.; Ellington, A. D.; Pishko, M. V.; Willson, C. G. *Chem. Mater.* **2004**, *16*, 5574−5580.

(9) Yeh, J. T. C.; Grebe, K. R. *J. Vac. Sci. Technol., A* **1983**, *1*, 604−608.

(10) Tacito, R. D.; Steinbrüchel, C. *J. Electrochem. Soc.* **1996**, *143*, 1974−1977.

(11) Renak, M. L.; Bazon, G. C.; Rotiman, D. *Adv. Mater.* **1997**, *9*, 392−395.

(12) Drury, C. J.; Mutsaers, C. M. J.; Hart, C. M.; Matters, M.; Leeuw, D. M. *Appl. Phys. Lett.* **1998**, *73*, 108−110.

(13) Kumar, A.; Whitesides, G. M. *Appl. Phys. Lett.* **1993**, *63*, 2002−2004.

(14) Kumar, A.; Whitesides, G. M. *Science* **1994**, *263*, 60−62.

(15) Xia, Y.; Zhao, X.-M.; Kim, E.; Whitesides, G. M. *Chem. Mater.* **1995**, *7*, 2332−2337.

(16) Xia, Y.; Tien, J.; Qin, D.; Whitesides, G. M. *Langmuir* **1996**, *12*, 4033−4038.

(17) Xia, Y.; Whitesides, G. M. *Langmuir* **1997**, *13*, 2059−2067.

(18) Xia, Y.; Mrksich, M.; Kim, E.; Whitesides, G. M. *J. Am. Chem. Soc.* **1995**, *117*, 9576−9577.

(19) St. John, P. M.; Craighead, H. G. *Appl. Phys. Lett.* **1996**, *68*, 1022−1025.

(20) Mrksich, M.; Whitesides, G. M. *Trends Biotechnol.* **1995**, *13*, 228−235.

(21) Chen, C. S.; Mrksich, M.; Huang, S.; Whitesides, G. M.; Ingber, D. E. *Science* **1997**, *276*, 1425−1428.

(22) Ostuni, E.; Chapman, R. G.; Liang, M. N.; Meluleni, G.; Pier, G.; Ingber, D. E.; Whitesides, G. M. *Langmuir* **2001**, *17*, 6336−6343.

(23) Hyun, J.; Zhu, Y.; Liebmann-Vinson, A.; Beebe, T. P., Jr.; Chilkoti, A. *Langmuir* **2001**, *17*, 6358−6367.

(24) Rowan, B.; Wheeler, M. A.; Crooks, R. M. *Langmuir* **2002**, *18*, 9914−9917.

(25) Suh, K. Y.; Seong, J.; Khademhosseini, A.; Laibinis, P. E.; Langer, R. *Biomaterials* **2004**, *25*, 557−563.

(26) Khademhosseini, A.; Suh, K. Y.; Jon, S.; Eng, G.; Yeh, J.; Chen, G.-J.; Langer, R. *Anal. Chem.* **2004**, *76*, 3675−3681.

(27) Berg, M. C.; Yang, S. Y.; Hammond, P. T.; Rubner, M. F. *Langmuir* **2004**, *20*, 1362−1368.

10.1021/la062268v CCC: $37.00
Published on Web 01/18/2007

jugated polymers,[31] metal particles,[32−38] and colloidal crystals.[39] Also, the chemically patterned reactive SAMs of thiols on gold or of silanes on silicon surfaces prepared by μCP can serve as templates for the directed growth of polymer thin films, in conjunction with a surface-initiated ring-opening metathesis polymerization (ROMP),[40,41] an underpotential deposition (UPD) of copper on gold followed by a surface-catalyzed polymerization,[42,43] an atom transfer radical polymerization (ATRP),[44] an electropolymerization,[45] or a chemical vapor deposition.[46,47]

The chemical vapor deposition (CVD) process is a useful method for the production of a variety of polymer coatings through the conversion of vaporized precursor monomers to polymeric films. Employing a one-step vacuum process that utilizes no solvent and no subsequent purification, uniform coatings of polymer thin films can be prepared on a variety of solid substrates including ones that present complex geometries with microscale features.[48] In addition, the CVD process enables certain monomers to be deposited as high-quality polymer films, that could not be attained by conventional solution-based polymerization routes which often result in decomposition or poor quality polymeric materials due to unfavorable reaction conditions or side reactions.[49] By the CVD process following μCP, we have previously demonstrated the selective growth of polymer films of poly(*p*-xylylene) (PPX, commercially known as parylene) and poly(*p*-phenylene vinylene) (PPV).[46,47] Specifically, we have employed certain transition metals, such as silver and iron, to inhibit the growth of PPX and PPV films in some patterning applications. Iron salts of chemically patterned SAMs of alkanethiols prepared by μCP have been used as templates for the selective growth of well-defined microscale patterns of PPX and PPV through a subsequent CVD process.

Isobenzofuran (IBF) was first isolated and characterized by Fieser and Haddadin.[50] IBF is highly reactive and in many synthetic pathways has been generated in situ as a transient intermediate. IBF has been used as a precursor for a variety of substituted naphthalenes and some heterocylic compounds.[49−52] We are currently investigating the development of polymeric forms of IBF for the development of new materials that have tunable optical, chemical, and electrical properties which can be utilized for diverse applications. Methods for the solution-based polymerization of IBF often result in many undesirable byproducts and low molecular weight polymers due to the very poor stability of IBF and its derivatives. Recently, we demonstrated that poly(isobenzofuran) (PIBF) can be prepared as high-quality polymer thin films by thermal CVD and hot-filament CVD (HFCVD) processes[53,54] and discovered that the growth of PIBF is surface-dependent. Specifically, the growth rate of PIBF films grown by the CVD process can be greatly affected by surface functional groups with different acidities present on the target substrates. This surface-dependent growth characteristic of PIBF films derived from a CVD process should enable the patterning of PIBF thin films.

In this paper, we present a method to direct the microstructure of PIBF thin films by a μCP−combined CVD process, based on the surface-dependent growth characteristics of PIBF. We investigate the growth rate, chemical structure, and composition of the PIBF films grown by thermal CVD on surfaces tailored with various functional groups of differing acidity, including a carboxylic acid (−COOH), a phenol (−PhOH), an alcohol (−OH), an amine ($-NH_2$), and a methyl ($-CH_3$) group. Based on the kinetic and spectroscopic analyses of these films, we prepared patterned SAMs of thiols on gold substrates that activate or deactivate regions of these surfaces; these templates enabled directed growth of PIBF by subsequent polymer CVD. As a part of our investigation, we employed carboxylic acid salts, including silver, iron, and copper salts, as the chemically reactive surfaces of the patterned SAMs, and examined the effect of these ions on the directed growth of PIBF by CVD.

Experimental Section

Materials. A precursor monomer, 1,2,3,4-tetrahydro-1,4-epoxynaphthalene, was synthesized according to the described synthetic procedure.[55,56] Silicon wafers (p-type, 100) were purchased from Montco Silicon Technologies, Inc. (Spring City, PA). All chemicals were purchased from Sigma-Aldrich Co. (St. Louis, MO). All chemicals were of reagent grade and used as received.

PIBF Growth onto SAMs of Thiols on Gold Substrates by CVD. The gold substrates were prepared by sequential deposition of titanium (5 nm at the rate of 2 Å/s) and gold (30 nm at the rate of 5 Å/s) onto silicon(100) surfaces in an electron beam evaporator. Gold substrates were soaked into 2 mM ethanolic solutions of 11-mercaptoundecanoic acid (MUA), 4-mercaptophenol, 11-mercapto-1-undecanol (MUO), 2-aminoethanethiol hydrochloride, and 1-undecanethiols (UDT) for 18 h to form SAMs. The modified gold substrates were then removed from the thiol solutions, rinsed with absolute ethanol, and dried under a stream of nitrogen prior to use. In order to investigate the effects of metal ions on the growth of PIBF by CVD, the surfaces of SAMs of MUA were associated with silver, iron, and copper ions. Carboxylic acid salts of these ions were prepared by dipping the SAMs of MUA on gold substrates into either an aqueous solution of silver sulfate (5 mM), iron(II) sulfate heptahydrate (10 mM), or copper(II) sulfate pentahydrate (10 mM)

(28) Jiang, X. P.; Zhang, H.; Gourding, S.; Hammond, P. T. *Langmuir* **2002**, *18*, 2607−2615.
(29) Park, J.; Kim, Y. S.; Hammond, P. T. *Nano Lett.* **2005**, *5*, 1347−1350.
(30) Li, H.; Kang, D.; Blamire, M. G.; Huck, W. T. S. *Nano Lett.* **2002**, *2*, 347−349.
(31) Liang, Z.; Li, K.; Wang, Q. *Langmuir* **2003**, *19*, 5555−5558.
(32) Jeon, N. L.; Nuzzo, R. G.; Xia, Y.; Mrksich, M.; Whitesides, G. M. *Langmuir* **1995**, *11*, 3024−3026.
(33) Jeon, N. L.; Clem, P. G.; Payne, D. A.; Nuzzo, R. G. *Langmuir* **1996**, *12*, 5350−5355.
(34) Palacin, S.; Hidber, P. C.; Bourgoin, J.-P.; Miramond, C.; Fermon, C.; Whitesides, G. M. *Chem. Mater.* **1996**, *8*, 1316−1325.
(35) Jeon, N. L.; Finnie, K.; Branshaw, K.; Nuzzo, R. G. *Langmuir* **1997**, *13*, 3382−3391.
(36) Jeon, N. L.; Lin, W.; Erhardt, M. K.; Girolami, G. S.; Nuzzo, R. G. *Langmuir* **1997**, *13*, 3833−3838.
(37) Zhong, Z.; Gates, B.; Xia, Y.; Qin, D. *Langmuir* **2000**, *16*, 10369−10375.
(38) Geissler, M.; Kind, H.; Schmidt-Winkel, P.; Michel, B.; Delamarche, E. *Langmuir* **2003**, *19*, 6283−6296.
(39) Yan, X.; Yao, J.; Lu, G.; Chen, X.; Zhang, K.; Yang, B. *J. Am. Chem. Soc.* **2004**, *126*, 10510−10511.
(40) Jeon, N. L.; Choi, I. S.; Whitesides, G. M.; Kim, N. Y.; Laibinis, P. E.; Harada, Y.; Finnie, K. R.; Girolami, G. S.; Nuzzo, R. G. *Appl. Phys. Lett.* **1999**, *75*, 4201−4203.
(41) Kim, N. Y.; Jeon, N. L.; Choi, I. S.; Takami, S.; Harada, Y.; Finnie, K. R.; Girolami, G. S.; Nuzzo, R. G.; Whitesides, G. M.; Laibinis, P. E. *Macromolecules* **2000**, *33*, 2793−2795.
(42) Guo, W.; Jennings, G. K. *Langmuir* **2002**, *18*, 3123−3126.
(43) Guo, W.; Jennings, G. K. *Adv. Mater.* **2003**, *15*, 588−591.
(44) Shah, R. R.; Merreceyes, D.; Husemann, M.; Rees, I.; Abbott, N. L.; Hawker, C. J.; Hedrick, J. L. *Macromolecules* **2000**, *33*, 597−605.
(45) Xia, C.; Advincula, R. C.; Baba, A.; Knoll, W. *Chem. Mater.* **2004**, *16*, 2852−2856.
(46) Vaeth, K. M.; Jensen, K. F. *Adv. Mater.* **1999**, *11*, 814−820.
(47) Vaeth, K. M.; Jackman, R. J.; Black, A. J.; Whitesides, G. M.; Jensen, K. F. *Langmuir* **2000**, *16*, 8495−8500.
(48) Pierson, H. O. *Handbook of Chemical Vapor Deposition*, 2nd ed.; Noyes Publications: Norwich, NY, 1999.
(49) Haddadin, M. J. *Heterocycles* **1978**, *9*, 865−901.
(50) Fieser, L. F.; Haddadin, M. J. *J. Am. Chem. Soc.* **1964**, *86*, 2081−2082.
(51) Warrener, R. N. *J. Am. Chem. Soc.* **1971**, *93*, 2346−2348.
(52) Rodrigo, R. *Tetrahedron* **1988**, *44*, 2093−2135.
(53) Choi, H.-G.; Amara, J. P.; Swager, T. M.; Jensen, K. F. *Macromolecules* **2006**, *39*, 4400−4410.
(54) Choi, H.-G.; Amara, J. P.; Martin, T. P.; Gleason, K. K.; Swager, T. M.; Jensen, K. F. *Chem. Mater.* **2006**, *18*, 6339−6344.
(55) Fieser, L. F.; Haddadin, M. J. *Can. J. Chem.* **1965**, *43*, 1599−1606.
(56) Wittig, G.; Pohmer, L. *Chem. Ber.* **1956**, *89*, 1334−1351.

Scheme 1. Formation and Polymerization of IBF by a Thermal CVD Process

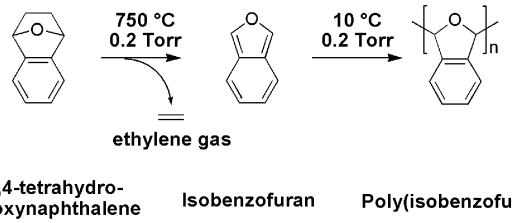

for 5 min[57] The surfaces were then rinsed for 20 s with a stream of deionized water and then dried under a stream of nitrogen. The polymer CVD system used in this study was described previously in detail.[53] As shown in Scheme 1, the precursor monomer (1,2,3,4-tetrahydro-1,4-epoxynaphthalene) was pyrolyzed at 750 °C and 0.2 torr to form IBF (the reactive monomer for the CVD polymerization), and PIBF films were then deposited onto the SAMs on gold substrates or onto the SAMs treated with the metal ions (Figure 1, parts a and b), at 10 °C and 0.2 torr.

Characterization of PIBF Films. The film thickness was measured by variable angle spectroscopic ellipsometry (VASE) with a J.A. Woollam M-2000s rotating compensator ellipsometer (J.A. Woollam Co., Inc, Lincoln, NE). The deposition was monitored in situ by interferometry using a 632.8 nm He−Ne laser (JDS Uniphase, San Jose, CA). A cycle thickness was calculated by dividing the total thickness of films by the number of cycles. Fourier transform infrared (FT-IR) spectra were obtained with a Nicolet Magna 860 spectrometer (Thermo Nicolet Corp., Madison, WI) in a reflection−absorption mode with an incident angle of 12° from the surface normal using a Harrick ERA12 accessory (Harrick Scientific Products, Inc., Pleasantville, NY), over the range of 400−4000 cm^{-1} at 4 cm^{-1} resolution. X-ray photoelectron spectroscopy (XPS) was used to monitor the surface composition of the PIBF films. XPS spectra were obtained with a Kratos Axis Ultra spectrometer (Kratos Analytical, Chestnut Ridge, NY) equipped with a monochromatized Al Kα X-ray source. Pass energies were 160 and 10 eV for survey and high-resolution scans, respectively. All peaks were fitted with 100% Gaussian, and the peak positions were referenced to C(1s) = 285.0 eV. The molecular weight of the PIBF film was measured by gel permeation chromatography (GPC) with a Waters 1525 binary high-performance liquid chromatography (HPLC) pump (Waters, Milford, MA) equipped with a R410 differential refractometer as a detector. All polymer films were dissolved in tetrahydrofuran (THF) and filtered through 0.45 μm syringe filters prior to use. Polystyrene standards from Aldrich were used for calibration and THF was used as the eluent. Optical microscopy images were obtained with an optical microscope (Nikon, TE300) equipped with a digital camera and an image processing software.

***μ*CP of Thiols on Gold Substrates and Subsequent PIBF Growth by CVD.** The deposition process of alkanethiols onto metal substrates by μCP has been discussed previously in detail.[47,58] The MUA and MUO inks were prepared as 2 mM solutions in absolute ethanol. As depicted in Figure 1, activation of regions of the gold substrates to promote PIBF growth was achieved by μCP of MUA or MUO on gold substrates (for 5−10 s) followed by backfill deposition of the remaining (surrounding) regions of gold substrates with a 2 mM ethanolic solution of UDT, which inhibits PIBF growth.

(57) The SAMs of MUA on gold substrates were soaked in a series of aqueous solutions of silver, iron, and copper with different concentrations and dipping times. The metal-associated surfaces were then analyzed by XPS to compare the intensity of Ag($3d_{5/2}$), Fe($2p_{3/2}$), and Cu($2p_{3/2}$). The intensities of high-resolution XPS spectra for each metal increased with increases in the concentration, and no further increases were observed from concentrations greater than 5, 10, and 10 mM for silver, iron, and copper, respectively. We also observed initial increases in XPS intensity with increased dipping time, and there was no significant difference in the XPS intensity from dipping times longer than 5 min. We determined these concentrations and the dipping time as the optimal conditions for the association of silver, iron, and copper onto the carboxylic acid-terminated SAMs.

(58) Kumar, A.; Biebuyck, H. A.; Whitesides, G. M. *Langmuir* **1994**, *10*, 1498−1511.

In order to investigate the effects of metal ions on the directed growth of PIBF by CVD, the patterned SAMs of MUA were also associated with silver, iron, and copper ions as described above. Subsequent depositions of PIBF were performed to fabricate microstructures of PIBF films either onto the patterned SAMs of MUA treated with the metal ions (Figure 1c) or onto the patterned SAMs of MUA or MUO (Figure 1d). The microstructures of the PIBF films were analyzed with a Nanoscope III atomic force microscope (Digital Instruments) in tapping mode.

Results and Discussion

Surface-Dependent Growth of PIBF by CVD. Figure 2 shows the FT-IR spectra of the PIBF films grown on carboxylic acid-, phenol-, alcohol-, amine-, and methyl-terminated surfaces. We observed that the PIBF films grown on carboxylic acid-, phenol-, and alcohol-terminated surfaces exhibit nearly identical absorption bands, which include the sp^2 C−H stretch from benzene ring at 3040 cm^{-1}, the sp^3 C−H stretch from the polymer backbone at 2874 cm^{-1}, the C═C aromatic stretch absorptions in a pair at 1597 and 1460 cm^{-1}, the furanoid C−O stretch absorptions in a pair at 1277 and 1035 cm^{-1}, the weak combination/overtone bands for the ortho-substituted benzene at 1670 and ∼1900 cm^{-1}, and the out-of-plane bending vibration for the ortho-substituted benzene at 755 cm^{-1}. These characteristic absorptions are consistent with those of typical PIBF films grown under the optimal operating conditions of PIBF CVD, i.e., T_v = 60 °C, T_p = 750 °C, T_s = 10 °C, and P = 0.2 torr, where subscripts v, p, and s represent vaporization, pyrolysis, and stage (deposition) temperatures, respectively.[53] On the other hand, we observed different absorption bands in the spectra of films grown on amine- and methyl-terminated surfaces. Specifically, the FT-IR spectra of the films grown on the methyl-terminated surfaces show dramatic decreases in the sp^2 C−H stretch from the benzene ring and the sp^3 C−H stretch from the polymer backbone. We also observed the decrease, shift, or disappearance of other absorptions, including the C═C aromatic stretch, the furanoid C−O stretch, the weak combination/overtone bands for the ortho-substituted benzene, and the out-of-plane bending vibration for the ortho-substituted benzene. These changes suggest that there may be a decrease in the degree of polymerization and the generation of different chemical structures during the film growth on these nonacidic surfaces, which indicates unfavorable polymerization conditions for the IBF.

XPS survey scans exhibited that the atomic composition of this set of PIBF films are similar to one another, typically 86.4% carbon and 13.6% oxygen. These values are consistent with the stoichiometry of PIBF, which possesses 85.7% carbon and 14.3% oxygen, respectively. However, the C(1s) high-resolution scans revealed that the films grown on amine- and methyl-terminated surface have slightly different atomic compositions from those grown on carboxylic acid-, phenol-, and alcohol-terminated surfaces (Figure 3a). Specifically, the spectra obtained from the PIBF films grown on the carboxylic acid-, phenol-, and alcohol-terminated surfaces show nearly identical features in the C(1s) region as observed from typical PIBF films. Each spectrum consists of two peak components corresponding to the aromatic carbons (i.e., *C*−C or *C*−H in the benzene ring) centered at 285.0 eV and the oxygen-bound carbon (i.e., *C*−O in the furanoid ring) centered at 286.7 eV. Area fractions of these peak components are typically 76.2% (*C*−C or *C*−H) and 23.8% (*C*−O), which is in good agreement with the stoichiometry of PIBF (75% *C*−C and 25% *C*−O). On the other hand, from the spectra of films grown on amine- and methyl-terminated surfaces, we observed that three peak components are present in C(1s) region, corresponding to *C*−C (285.0 eV), **C* (285.7 eV), and

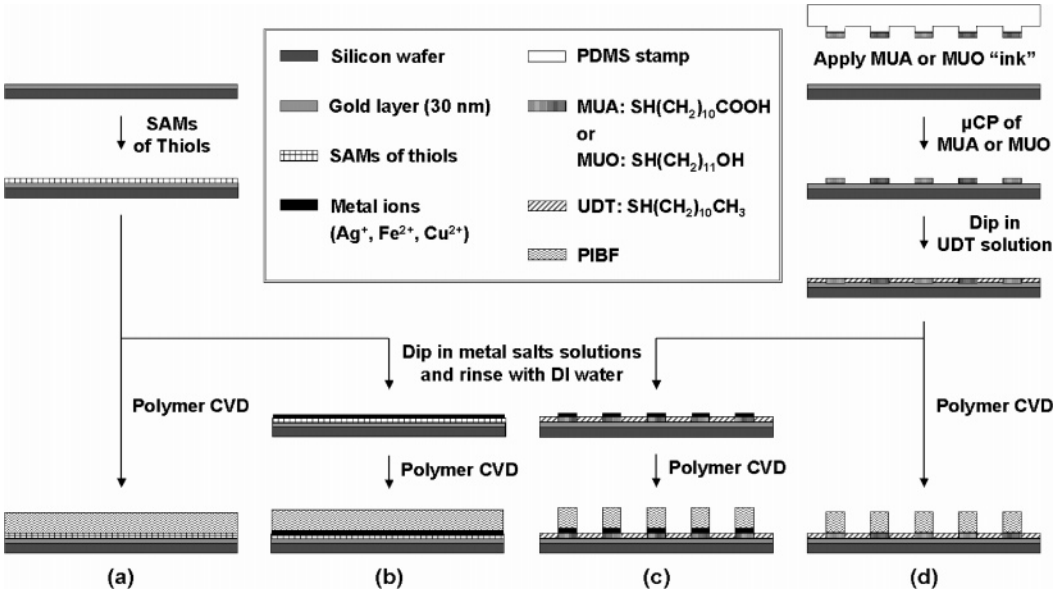

Figure 1. PIBF growth by CVD (a) on self-assembled monolayers (SAMs) of 5 different thiols (i.e., MUA, 4-mercaptophenol, MUO, 2-aminoethanethiol hydrochloride, and UDT) on gold substrates, (b) on carboxylic acid-terminated SAMs (MUA) treated with metal ions (Ag^+, Fe^{2+}, and Cu^{2+}), (c) on patterned SAMs of MUA treated with metal ions (Ag^+, Fe^{2+}, and Cu^{2+}), and (d) on patterned SAMs of MUO or MUA.

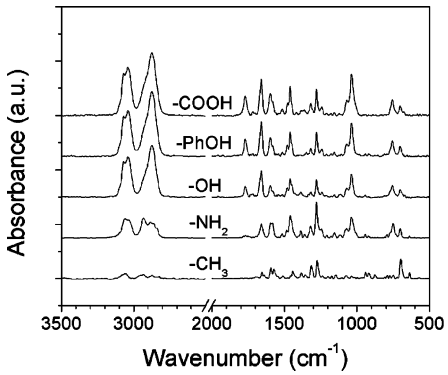

Figure 2. Reflection−absorption FT-IR spectra of PIBF films grown on carboxylic acid-, phenol-, alcohol-, amine-, and methyl-terminated self-assembled monolayers (SAMs) on gold substrates.

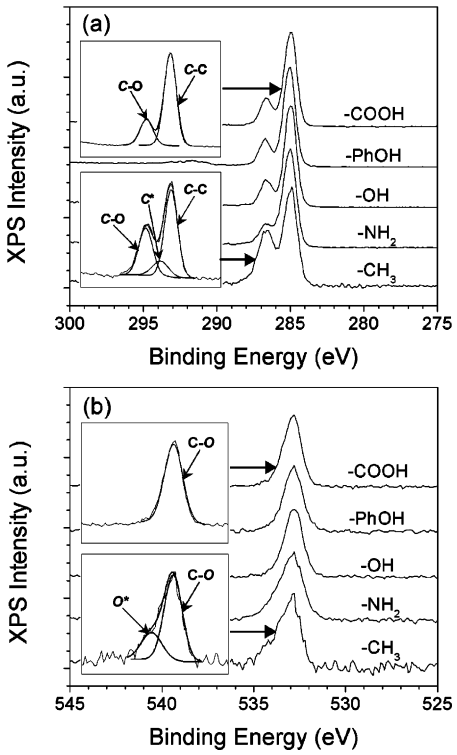

Figure 3. High-resolution XPS spectra of (a) C(1s) and (b) O(1s) obtained from the PIBF films grown on carboxylic acid-, phenol-, alcohol-, amine-, and methyl-terminated self-assembled monolayers (SAMs) on gold substrates.

C−O (286.7 eV), respectively. This new peak component at 285.7 eV is usually assigned as a carbon adjacent to either a carboxyl or an ester group (i.e., *C*−COOR) when it appears along with their carbonyl peak components centered typically at 288.5−289.3 eV.[59] However, we observed no sign of a carbonyl peak component in C(1s) region. Another possibility for the generation of this new peak component could be an inclusion of ketal (acetal) groups in the films, but we can also neglect this possibility because there is no sign of ketals in the C(1s) region as well, which should appear in the higher binding energy region, i.e., ∼288.2 eV.

From the high-resolution O(1s) spectra of the polymer films (Figure 3b), we observed that only the single peak component (centered at 532.9 eV with fwhm of 1.2 eV) is present in the films grown on carboxylic acid-, phenol-, and alcohol-terminated surfaces while two peak components exist in the films grown on amine- and methyl-terminated surfaces. These two peak components correspond to C−*O* (532.9 eV) that is nearly identical to the single-peak component present in typical PIBF films and a new peak, **O* (533.8 eV). Because the binding energy of the oxygen atom of the carbonyl group usually appears around 532.3 eV (for an aliphatic compound) or 531.3 eV (for an aromatic compound),[59] this new peak component centered at 533.8 eV cannot be considered to be an oxygen atom from a carbonyl group but could be an oxygen atom bound to a different functional group.

We speculate that the generation of these new peaks centered at 285.7 eV in C(1s) region and at 533.8 eV in O(1s) region could be due to carbons attached to another type of C−O bond

(59) Beamson, G.; Griggs, D. *High Resolution XPS of Organic Polymers: The Scienta ESCA300 Database*; John Wiley & Sons: New York, 1992; pp 277−292.

Table 1. Analyses of the C(1s) and O(1s) High-Resolution XPS Spectra of PIBF Films Grown on Different Surfaces[a]

	C(1s) composition (%)			O(1s) composition (%)	
surface functional groups	*C*−C (BE: 285.0 eV)	*C** (BE: 285.7 eV)	*C*−O (BE: 286.7 eV)	C−*O* (BE: 532.9 eV)	*O** (BE: 533.8 eV)
−COOH	76.2		23.8	100.0	
−PhOH	76.4		23.6	100.0	
−OH	76.7		23.3	100.0	
$-NH_2$	76.8	6.5	16.7	73.6	26.4
$-CH_3$	55.7	11.9	32.4	72.5	27.5

[a] Full width at half-maximum (fwhm) of each peak component in the C(1s) and O(1s) regions were defined as 1.0 and 1.2 eV, respectively, for curve fitting to resolve these spectra.

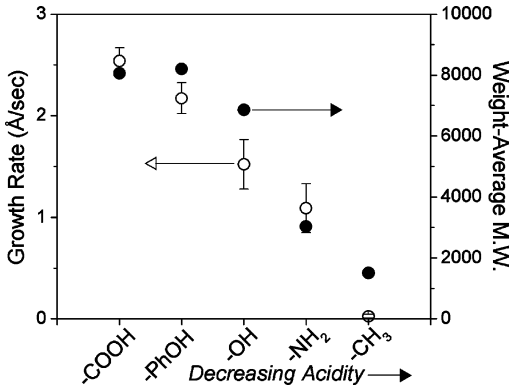

Figure 4. Growth (deposition) rate (○) and weight-average molecular weight (●) of PIBF films grown on carboxylic acid-, phenol-, alcohol-, amine-, and methyl-terminated surfaces.

present in the polymerization byproducts that are suspected to have different chemical structures from PIBF. Area fractions of the peak components in the C(1s) and O(1s) regions for this set of films are summarized in Table 1. These results are quite similar to those obtained from PIBF films containing disordered dendritic defects or different materials as byproducts, which we prepared, in a previous work, under low vaporization temperatures ($T_v \leq$ 50 °C) or high pyrolysis temperatures ($T_p \geq$ 800 °C); both conditions can promote different reaction pathways for IBF by providing excess thermal energy in the pyrolysis zone.[53]

From the ellipsometry analysis, we find that this set of films have approximately the same thickness (∼650 nm), except for the films grown on methyl-terminated surfaces. Using interferometry data, we calculated the growth rate of the PIBF films and compared them with respect to the acidity of the surface functional groups. Figure 4 presents the trend in PIBF growth rates versus the pK_a of these surface functional groups in an order of decreasing acidity along the *X*-axis. We observed the fastest growth of PIBF ($k = 2.5$ Å/s) on the carboxylic acid-terminated surfaces, whereas films on the methyl-terminated surfaces exhibited very slow growth ($k = 0.02$ Å/s). Overall, the growth rate of PIBF films decreased with the decrease in acidity of the surface functional groups. Additionally, GPC analysis of this set of polymer films revealed that the weight-average molecular weights of PIBF grown on carboxylic acid- and phenol-terminated surfaces were around 8000 and decreased to 1500 as the acidity of the surface functional group decreased (Figure 4), which is well consistent with the trend in growth rate. These results are evidence that the PIBF growth can follow a cationic polymerization mechanism as acidic environments promote the initiation of polymerization by providing Brønsted acids or Lewis acids as cationic initiators in polymerization reactions. Besides the acidic environment, the reaction temperature for polymerization, i.e., surface (deposition) temperature in the CVD polymerization process, is another critical parameter in a cationic polymerization.[60] It is known that propagation in a cationic polymerization is a rapid and an exothermic process, and therefore the reaction temperature should be low to facilitate the polymerization. In our previous work, we revealed that the control of the surface (deposition) temperature in the CVD process for the polymerization of IBF is very important to achieve fast growth of PIBF films as well as to obtain a high-quality polymeric coating. Specifically, the growth rate of PIBF is decreased with the increase in the surface temperature,[53] which is well consistent with the role of reaction temperature in a cationic polymerization.

Figure 5 shows optical microscope images of PIBF films grown on SAMs with different surface functional groups. We observed that the films grown on carboxylic acid-, phenol-, and alcohol-terminated surfaces are defect-free (Figure 5a−c), whereas disordered dendritic defects and discontinuous growth (i.e., island-like growth) appear in the films grown on the amine-terminated (Figure 5d) and methyl-terminated (Figure 5e) surfaces, respectively. By AFM analysis, we observed that small grains (average size of ∼40 nm and average rms roughness of ∼0.35 nm) coalesce to form continuous layers of PIBF in the defect-free films grown on carboxylic acid-, phenol-, and alcohol-terminated surfaces (data not shown). On the other hand, the films grown on amine-terminated surfaces have two distinctive domains, PIBF and defect domains. The PIBF domain showed similar morphologies to those observed in the defect-free films, whereas the defect domain exhibited much rougher surface morphology (average rms roughness of ∼400 nm). These results are quite similar to those obtained from PIBF films prepared under low vaporization temperatures ($T_v \leq$ 50 °C) or high pyrolysis temperatures ($T_p \geq$ 800 °C),[53] which contain dendritic or disordered dendritic defects, although there is quite a large difference in the rms roughness. As described in our previous work, the reactive IBF monomer is deactivated upon adsorption to surfaces with unfavorable reaction environments, i.e., nonacidic surfaces in this case. The deactivated regions can inhibit the initiation and propagation of PIBF growth and develop into defect domains. Nonetheless, there is a possibility for secondary adsorption of the active species onto the defect domain if the delivery rate of the active species is high enough to overcome the deactivation rate of the adsorbing active species. We speculate that the PIBF domain formed on the amine-terminated surface could be due to the polymer nucleation induced by this secondary adsorption process of the active species of IBF monomer. The presence of the PIBF domain in these films is supported by the characteristic absorption bands of PIBF in the FT-IR spectrum, although there is a decrease in the peak intensity of the sp^3 C−H stretch from the polymer backbone (Figure 2), indicating a decrease in the degree of polymerization, as evidenced by the low molecular weight

(60) Odian, G. *Principles of Polymerization*, 4th ed.; John Wiley & Sons, Inc.: NJ, 2004; Chapter 4.

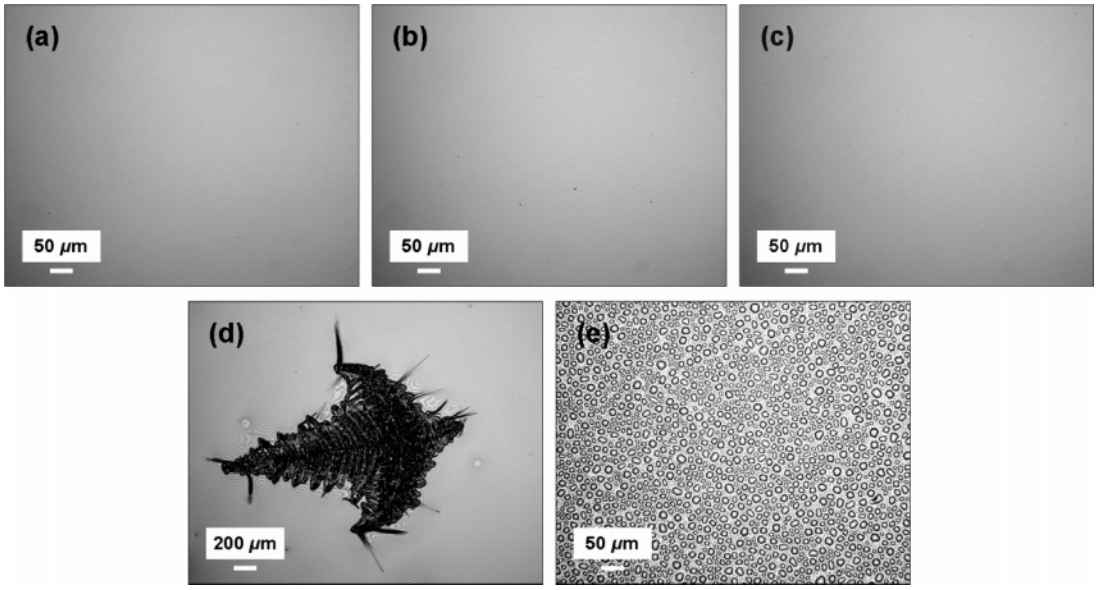

Figure 5. Optical microscope images of PIBF films grown on (a) carboxylic acid-, (b) phenol-, (c) alcohol-, (d) amine-, and (e) methyl-terminated SAMs.

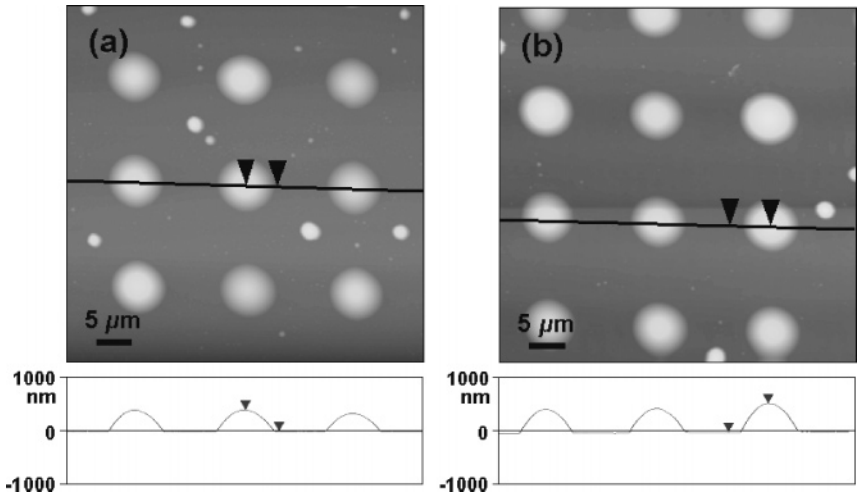

Figure 6. AFM images of microstructures of PIBF films grown on (a) the patterned SAMs of MUO (alcohol-terminated alkanethiol) and (b) the patterned SAMs of MUA (carboxylic acid-terminated alkanethiol), in which all surrounding (background) regions were coated with SAMs of UDT (methyl-terminated alkanethiol) prior to the deposition of PIBF. The feature size is 6 μm in diameter. The average thickness of the microstructures is 400 and 490 nm for the PIBF films grown on the patterned SAMs of MUO and MUA, respectively. All images were obtained by tapping mode with a 0.5 Hz scan rate and a 50 μm $\times$ 50 μm scan size.

($\sim$3000) from the GPC analysis. We also observed that the films eventually grow on the methyl-terminated surface, with discontinuous, island-like patterns. However, these films are quite different in chemical structure and molecular weight as supported by the FT-IR (Figure 2) and GPC analysis (Figure 4). We speculate that the films grown on the methyl-terminated surfaces consist of small molecules or oligomers with different chemical structures from PIBF. These materials are produced through different reaction pathways induced by the unfavorable deposition environments of the nonacidic surfaces.

Directed Growth of PIBF on Patterned SAMs. Using μCP, we prepared the patterned SAMs on gold substrates that have two distinct regions; one region facilitates PIBF growth while the other region inhibits PIBF growth. Based on the growth behavior of PIBF on the various SAM surfaces, we prepared surfaces patterned with SAMs of MUO and MUA, in which the surrounding (background) regions were coated with UDT, so as to direct the formation of the microstructures of PIBF to the areas with MUO or MUA. Another reason that we selected MUO and MUA is that the length of these molecules is comparable to that of the surrounding SAMs (UDT). The similar length of these molecules helps to prevent possible bias that can result from a height difference between the patterned regions and surrounding regions in the initial stage of PIBF deposition. Figure 6 shows AFM images of the microstructures of PIBF grown on the patterned SAMs of MUO and MUA. As can be expected from the initial SAM results, PIBF films grew selectively on the regions patterned with MUO and MUA. The feature size of these microstructures of PIBF is 6 μm in diameter, which is in good agreement with the feature size of the stamp used for the μCP (6 μm patterned circles). The average thicknesses of the selectively grown microstructures are 400 and 490 nm for PIBF grown on the patterned SAMs of MUO and MUA, respectively. The difference in the microstructure thickness between these two SAMs is due to the different growth rates of PIBF on MUO and MUA, as shown in Figure 4. Small features with sizes up to 2 μm might be due to the secondary nucleation of PIBF at some locations of the UDT-coated regions or to PIBF growth at some

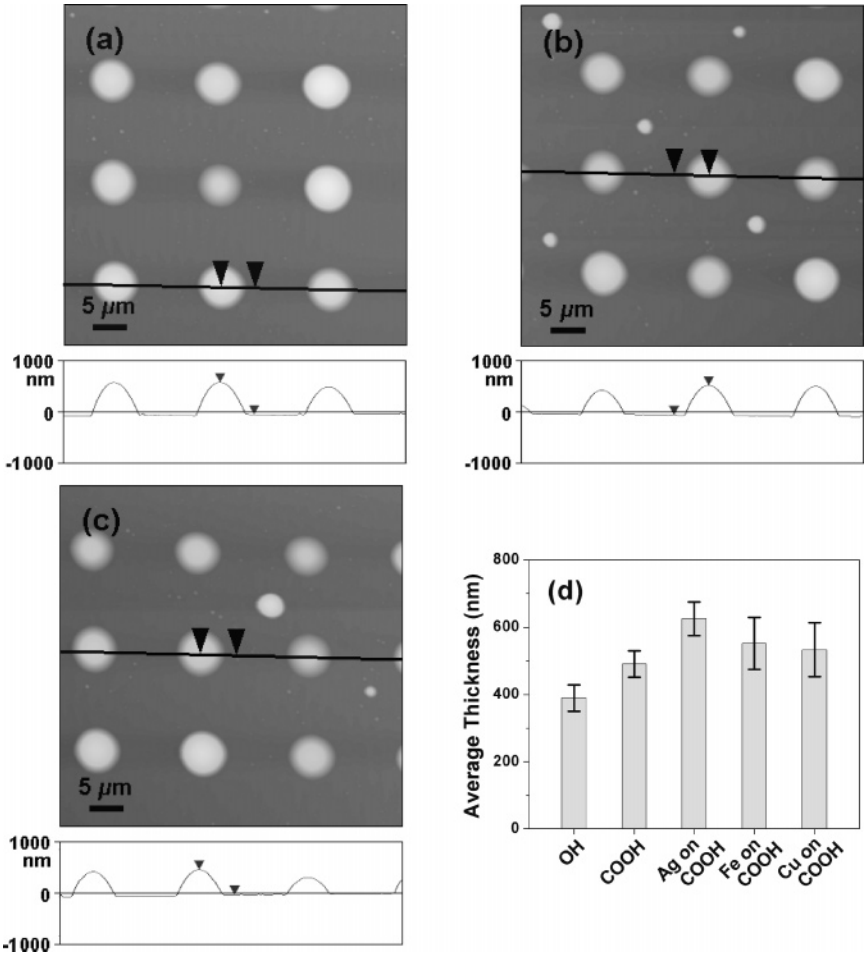

Figure 7. AFM images of the microstructures of PIBF grown on the patterned SAMs of MUA that had been treated with (a) 5 mM Ag_2SO_4 for 5 min, (b) 10 mM $FeSO_4 \cdot 7H_2O$ for 5 min, and (c) 10 mM $CuSO_4 \cdot 5H_2O$ for 5 min. The feature sizes average 6 μm in diameter. All images were obtained by tapping mode with a 0.5 Hz scan rate and a 50 μm $\times$ 50 μm scan size. (d) The average thickness of the microstructures of PIBF grown on the various surfaces is presented for comparison.

locations in the surrounding (background) regions that are supposed to be coated with UDT in the later step of the μCP process (backfill deposition) but could have been coated with MUO or MUA during the μCP (i.e., incomplete μCP of MUO or MUA). The selectivity of PIBF growth on the patterned SAMs could be maintained until the average thickness of microstructures reach up to 400 nm on alcohol-terminated surface and 500 nm on carboxylic acid-terminated surface with less than 0.5% of surface coverage of defects.

Effects of Metal Ions on PIBF Growth by CVD. In order to investigate the effects of various metal ions on the growth of PIBF, we performed CVD of PIBF onto the patterned SAMs of MUA that were associated with metal ions (Ag^+, Fe^{2+}, and Cu^{2+}), as depicted in Figure 1c. With the use of SAMs patterned with MUA by μCP, these metal ions can be readily directed to certain locations on the SAM surface through the formation of carboxylic acid salts. Figure 7 shows AFM images of the microstructures of PIBF grown on the patterned SAMs of MUA treated with Ag^+, Fe^{2+}, and Cu^{2+}, respectively. We observed that the microstructures of the PIBF also grow selectively on the patterned SAMs of MUA associated with the metal ions. These results are in contrast to the previously reported behavior of both parylene (PPX) and PPV, in which selective growth of parylene and PPV was achieved through inhibition of the polymer growth by the metals or metal ions (iron, silver, copper, ruthenium, platinum, and palladium).[46,47] The selective growth of PIBF on the metal ion-associated, patterned SAMs of MUA could be explained by the combined effect of the higher surface energy of the metal-associated regions of the SAMs of MUA and also the presence of residual carboxylic acid groups as a result of the incomplete association of the metal ions. The higher surface energy of the metal-associated region could provide better adsorption for the active species of the adsorbing monomer, and the residual carboxylic acid groups could serve as initiators for cationic polymerization and for the formation of microstructures of PIBF.

In all cases (Figure 7−c), the feature size of the microstructures of PIBF averages 6 μm in diameter, which is in good agreement with the geometry of the stamp used for the μCP (6 μm patterned circles). Compared to the average thickness of the microstructures grown on the patterned SAMs of MUA (490 nm), we observed relative increases in the range of 10−27% in the thicknesses of the PIBF films grown on the metal ion-associated, patterned SAMs. Considering that these surfaces can all serve as cationic initiators for the polymerization of IBF, the differences in thickness might be explained through differences in the surface energy between the various surfaces. The metal-associated surfaces could demonstrate better adsorption efficiency for the IBF monomers than the patterned SAMs of MUO or MUA, due to their higher surface energies compared to those of the organic surfaces. Consequently, the initiation and the propagation of the polymerization would be more favorable on the metal ion-associated surfaces than on the organic SAMs, resulting in increases in the growth rate and the thickness of the PIBF microstructures. In cases of metal ion-associated surfaces, the

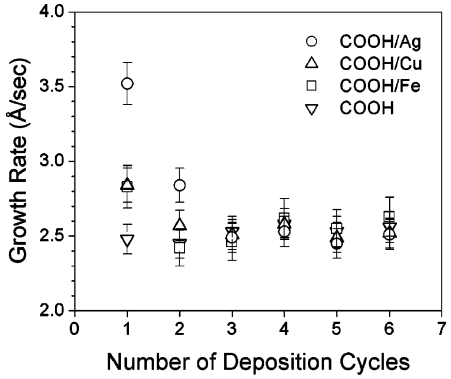

Figure 8. Growth rate of PIBF as a function of time (i.e., the number of deposition cycles) on SAMs of MUA treated with Ag^{+} (○), Fe^{2+} (□), and Cu^{2+} (△). The growth rate of PIBF on untreated SAMs of MUA (▽) was included as a control.

selectivity of PIBF growth could be maintained until the average thickness of microstructures reach up to 625, 550, and 535 nm for silver, iron, and copper salts treated surfaces, respectively, with less than 0.5% of surface coverage of defects.

We also observe that the average thickness of the microstructures is dependent on the metal species associated with the carboxylic acid groups on the patterned SAMs of MUA (i.e., 625, 550, and 535 nm for silver, iron, and copper salts, respectively), as shown in Figure 7d. In order to investigate the growth dependence of PIBF on these metal species, we have analyzed the growth rate of PIBF by in situ interferometry. The growth rate of PIBF for each deposition cycle was calculated by dividing the cyclic thickness (typically 110 nm) by the cyclic period of each case. As shown in Figure 8, the PIBF films grown on the carboxylic acid-terminated surfaces exhibit nearly the same growth rate during the entire deposition process (i.e., $k \sim$ 2.50 Å/s). On the other hand, the PIBF films grown on the metal-associated carboxylic acid surfaces demonstrate a somewhat faster growth rate than the untreated surfaces, especially in the early stages of deposition, such as the first or the second cycle. For iron- and copper-associated surfaces, the growth rates of the PIBF in the first cycle of the deposition were 2.83 and 2.84 Å/s, respectively. From the second cycle of deposition, the iron- and the copper-associated surfaces exhibited similar growth rates to that of the carboxylic acid-terminated surfaces. The average growth rates of the PIBF films on the iron- and copper-associated surfaces, at this period, were 2.54 and 2.53 Å/s, respectively. These results indicate that the nucleation effect on the PIBF growth is dominant during the first cycle of deposition, which could be the result of the higher surface energy of the metal-associated surfaces than the organic surfaces, such as the carboxylic acid-terminated surfaces. In the case of the silver-associated surfaces, the faster growth rates of the PIBF films were retained until the second cycle of the deposition, although the growth rate decreased with increase in the number of deposition cycles and reached similar growth rates to that of the carboxylic acid-terminated surfaces from the third deposition cycle on. These differences in the growth rates from the iron- or copper-associated surfaces indicate that the silver-associated surfaces can present not only a nucleation effect but, perhaps, make an additional contribution to the PIBF growth through a catalytic effect that is similar to facilitating polymer growth in surface-initiated polymerizations.

In order to verify the additional positive effects of the silver ions on the PIBF growth, we examined the relative amount of the silver ions present on the surfaces of the growing PIBF as a function of the deposition cycle, by means of measuring the

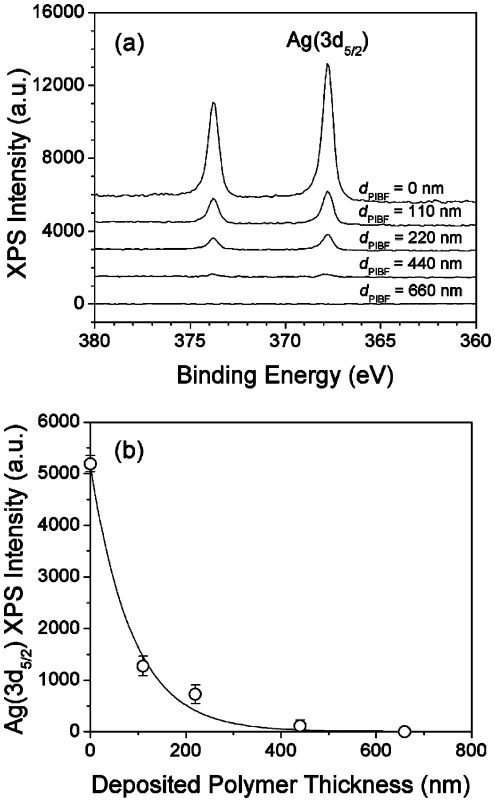

Figure 9. (a) $Ag(3d_{5/2})$ high-resolution XPS spectra of PIBF films grown on silver-associated surfaces of SAMs of MUA and (b) its intensity as a function of the thickness of PIBF films.

peak intensity of $Ag(3d_{5/2})$ in the high-resolution XPS spectra. Since XPS can only detect the photoelectrons emitted from atoms present within a few nanometers of the film surfaces, XPS signals of $Ag(3d_{5/2})$ from the PIBF-deposited surfaces suggest that the silver atoms could be present at the very surface of the PIBF film, or at least in the region within a few nanometers from the surface. From the silver-associated surfaces deposited with different thicknesses of PIBF, we observed that the XPS intensity of $Ag(3d_{5/2})$ decreases with increase in the thickness of the deposited PIBF films (Figure 9a). Integration of these peaks can provide a trend of the relative amount of silver ions present on the surface of the various PIBF films (Figure 9b). Specifically, the relative amount of silver ions on the surfaces of 110 and 220 nm thick PIBF films (110 nm corresponds to one deposition cycle) decreased to 24.5% and 13.8% of the amount of silver ions on the control surface, i.e., silver-associated surfaces without PIBF films. This amount reached zero when the thickness of the deposited PIBF films was greater than 440 nm (four cycles of deposition). On the other hand, the XPS intensity of $Fe(2p_{3/2})$ or $Cu(2p_{3/2})$ is almost the same, essentially zero, over the course of the PIBF deposition onto iron- or copper-associated surfaces (data not shown). These differences could result from the weaker binding affinity of the silver ions to the surface functional groups (carboxylic acids) on SAMs of MUA than that of iron or copper ions to the surfaces of SAMs containing the same functional groups. Based on the XPS analysis, we speculate that some portion of the silver ions from the carboxylic acid salts of MUA can dissociate due to their weaker binding affinity and move in the direction of the polymer growth. These silver ions can serve to facilitate PIBF growth. This additional contribution to the PIBF growth rate would remain until the migration of the silver ions toward outer surfaces becomes negligible, i.e., after the third cycle of deposition in this case (Figure 8).

Conclusions

Chemical vapor deposition (CVD) of poly(isobenzofuran) (PIBF) films on self-assembled monolayers (SAMs) of various thiols on gold substrates with different surface functional groups reveals that the growth of PIBF is surface-dependent and undergoes a cationic polymerization mechanism. We observed the fastest growth of PIBF on carboxylic acid-terminated SAMs ($k = 2.5$ Å/s), whereas films grew slowly on methyl-terminated SAMs ($k = 0.02$ Å/s). The surface-dependent growth characteristics of PIBF facilitated the development of the microcontact printing (μCP)−combined CVD process for the patterning of PIBF thin films. This process was found to be an effective method for the directed formation of microstructures of PIBF with good spatial resolution. The association of various metal ions onto the carboxylic acid groups of the chemically patterned SAMs provided a useful method for the improvement of the thickness of the microstructures of PIBF.

The described process has advantages over other patterning methods. These advantages include that the exposure of the polymeric layers to solvents is not required for pattern formation and that no additional processing steps are needed to refine the polymeric patterns. Additionally, the feature sizes that can be produced are comparable to those used in electronic circuits, display panels, and microarrays used for biosensors. With the use of specially designed precursor monomers, the μCP−combined CVD process for the directed growth of PIBF may offer a simple and flexible means to construct microstructures that can be used as sensing elements in microfluidic devices for biological applications.

Acknowledgment. This work was supported by the U.S. Army through the Institute for Soldier Nanotechnologies (ISN), under the Contract (DAAD-19-02-0002) with the U.S. Army Research Office and in part by the MRSEC Program of the National Science Foundation under the Award No. DMR 02-13282. T.M.S. acknowledges support from the Office of Naval Research MURI program.

LA062268V